Science Advances
AAAS

advances.sciencemag.org/cgi/content/full/6/16/eaax9757/DC1

Supplementary Materials for

A highly sensitive and selective nanosensor for near-infrared potassium imaging

Jianan Liu, Limin Pan, Chunfeng Shang, Bin Lu, Rongjie Wu, Yun Feng, Weiyu Chen, Rongwei Zhang, Jiwen Bu, Zhiqi Xiong*, Wenbo Bu*, Jiulin Du*, Jianlin Shi*

*Corresponding author. Email: forestdu@ion.ac.cn (J.D.); wbbu@chem.ecnu.edu.cn (W.B.); xiongzhiqi@ion.ac.cn (Z.X.); jlshi@mail.sic.ac.cn (J.S.)

Published 17 April 2020, *Sci. Adv.* **6**, eaax9757 (2020)
DOI: 10.1126/sciadv.aax9757

The PDF file includes:

Other Supplementary Material for this manuscript includes the following:

(available at advances.sciencemag.org/cgi/content/full/6/16/eaax9757/DC1)

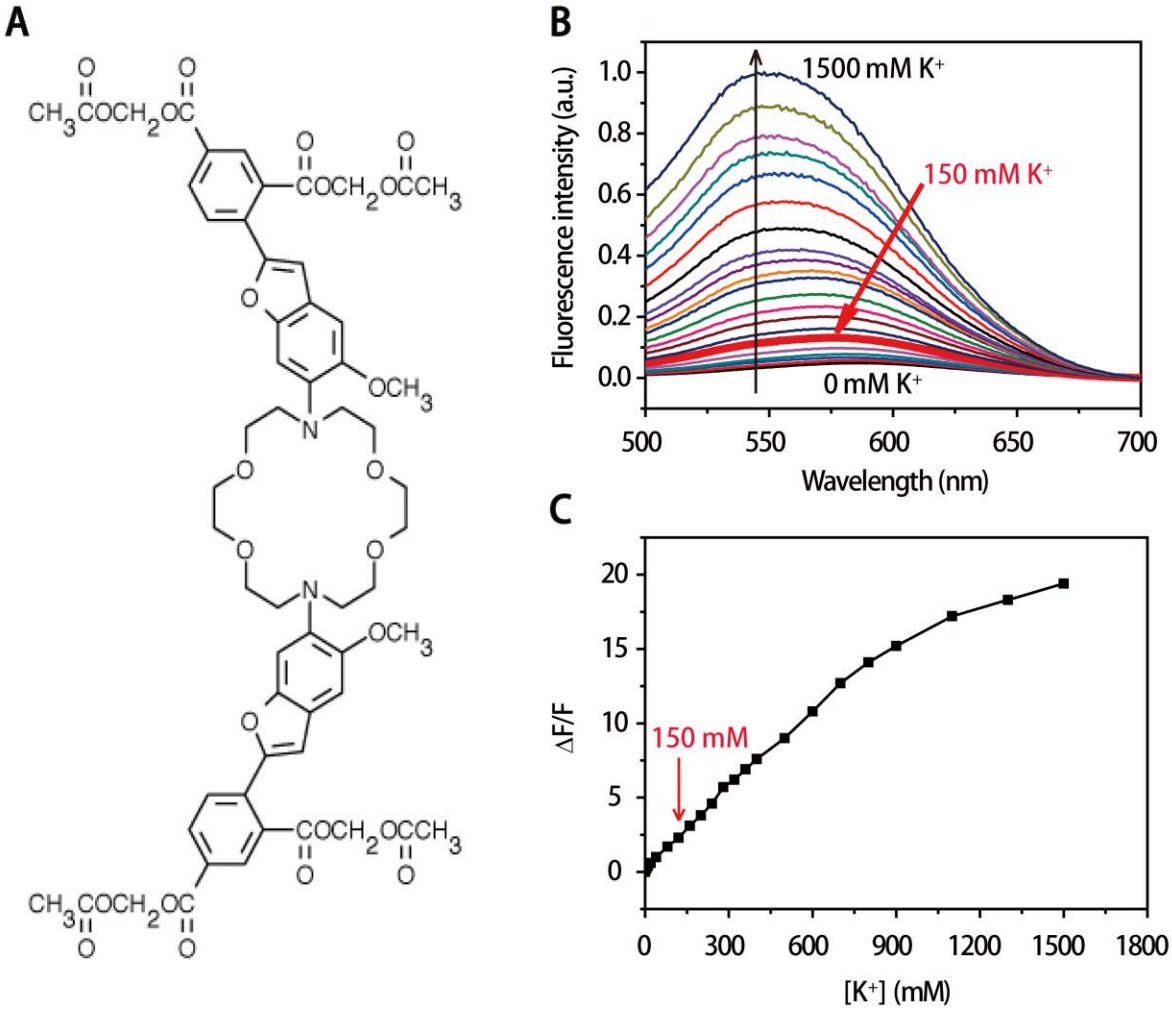

Fig. S1. The structure and K^+ sensing performance of PBFI. (A) Chemical structure of the potassium indicator PBFI. **(B)** Fluorescence changes of PBFI in HEPES buffer (pH 7.2) containing different KCl concentrations, excited at 365 nm. **c**, Fluorescence fluctuations at 540 nm at different K^+ concentrations. F is the fluorescence intensity at various conditions, and ΔF is its change.

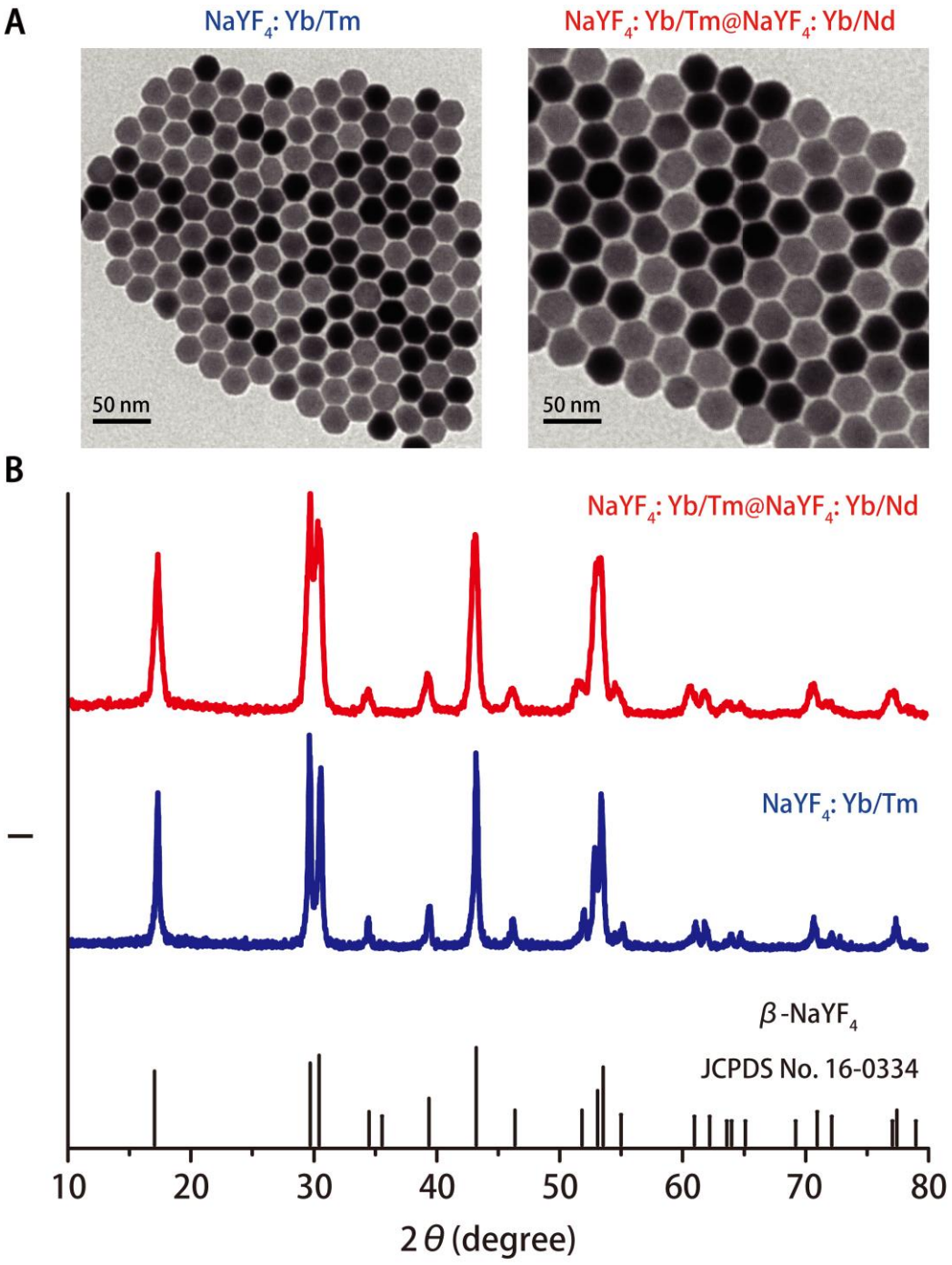

Fig. S2. Characterization of UCNPs. (A) TEM images of $NaYF_4$: Yb/Tm and $NaYF_4$: Yb/Tm@$NaYF_4$: Yb/Nd nanoparticles. **(B)** XRD patterns of the collected solid $NaYF_4$: Yb/Tm and $NaYF_4$: Yb/Tm@$NaYF_4$: Yb/Nd nanoparticles.

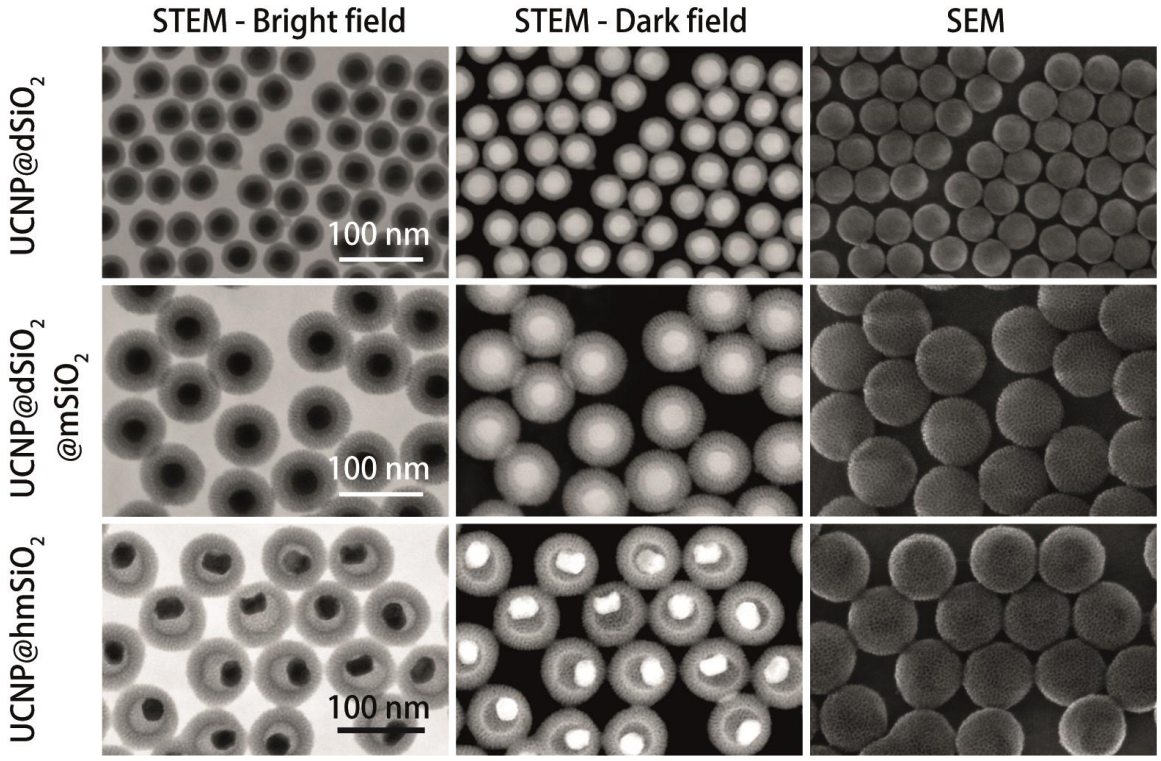

Fig. S3. Structure characterization of various nanoparticles in the growth pathway of nanosensors. Bright/dark field scanning transmission electron microscopy (STEM) and scanning electron microscopy (SEM) images of UCNP@$dSiO_2$, UCNP@$dSiO_2$@$mSiO_2$, and UCNP@$hmSiO_2$, respectively.

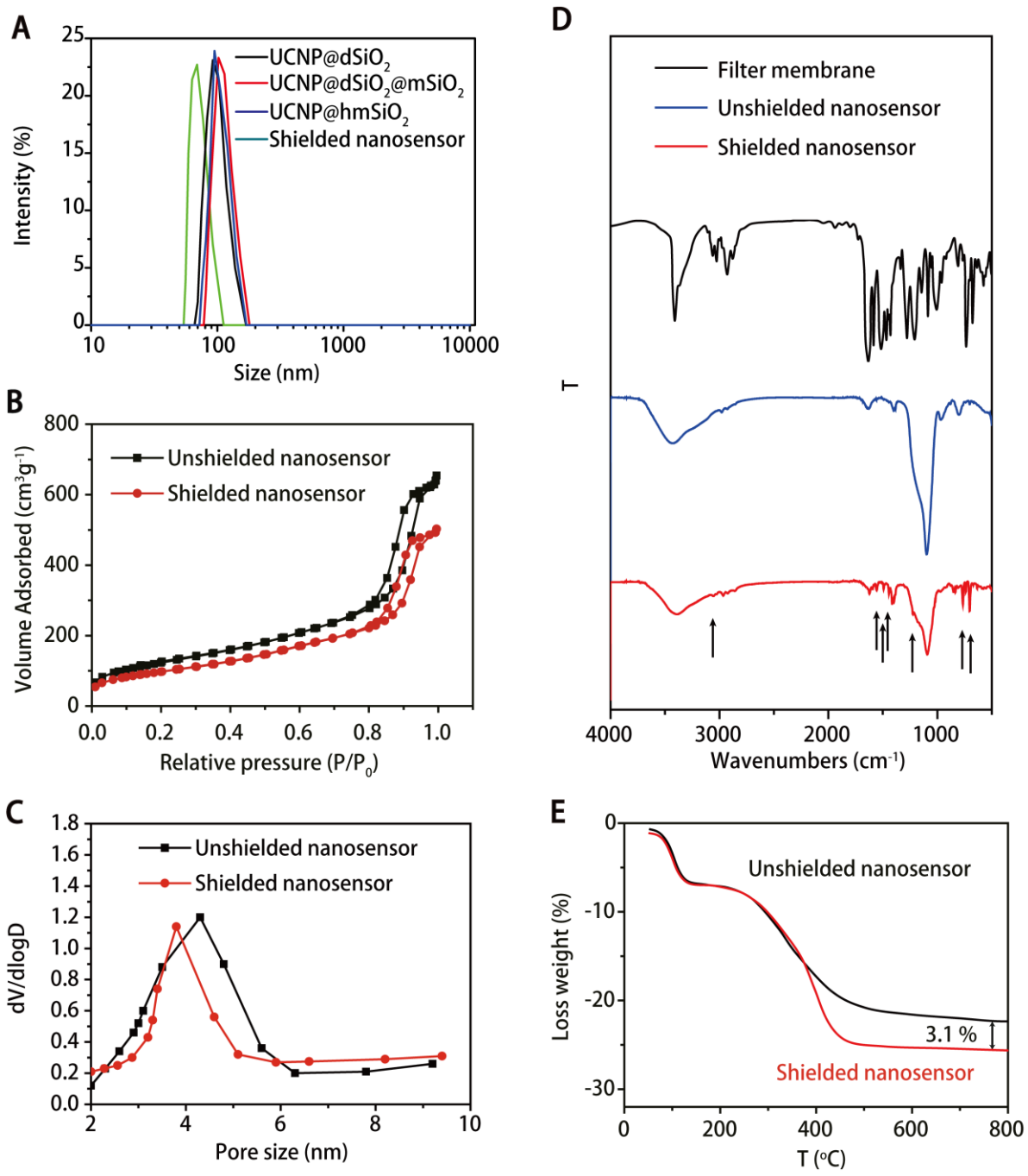

Fig. S4. Characterization of both shielded and unshielded nanosensors. (A) Size distribution plot for UCNP@dSiO$_2$, UCNP@dSiO$_2$@mSiO$_2$, UCNP@hmSiO$_2$, and shielded nanosensors. **(B)** Nitrogen adsorption–desorption isotherms of the unshielded/shielded nanosensors. **(C)** Pore size distributions of the unshielded/shielded nanosensors. **(D)** The appearance of new chemical bondings after filter membrane shielding as marked with black arrows. **(E)** Thermogravimetric analysis plots of the unshielded/shielded nanosensors.

Table S1. Summary of pore structure parameters for UCNP@hmSiO_2 and the filter membrane-shielded UCNP@hmSiO_2.

Materials	**BET (m^2/g)**	**Pore volume (cm^3/g)**	**Pore size distribution (nm)**
UCNP@hmSiO_2	554.5	1.03	4.3
filter membrane-shielded UCNP@hmSiO_2	382.7	0.72	3.8
filter membrane-shielded UCNP@hmSiO_2 after 20 cycles of [K^+] increase	316.3	0.55	3.1

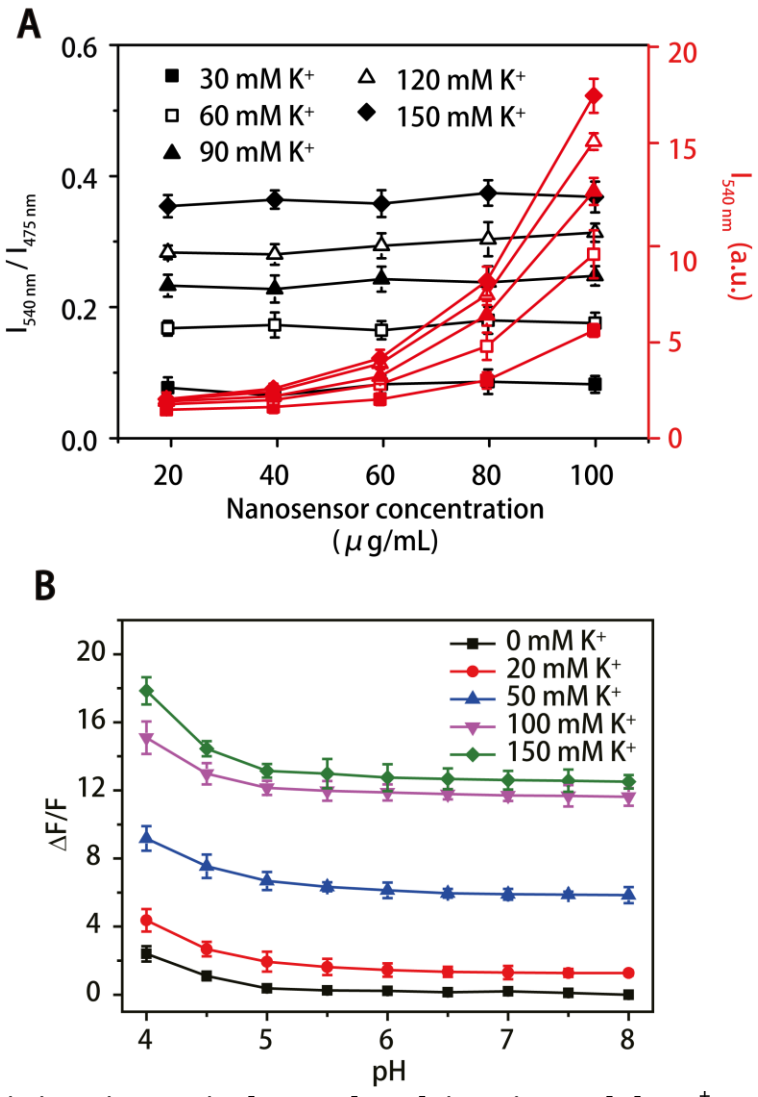

Fig. S5. Ratiometric imaging vs single-wavelength imaging and the K^+ sensing performance of the shielded nanosensors under various pH values. (A) Nanosensor concentration-dependent UCL emission (540 nm) and nanosensor concentration-independent ratio ($I_{540\ nm}/I_{475\ nm}$) under varied [K^+]. **(B)** Nanosensor fluorescence as a function of solution pH at indicated [K^+] (error bars represent s.d., n = 3).

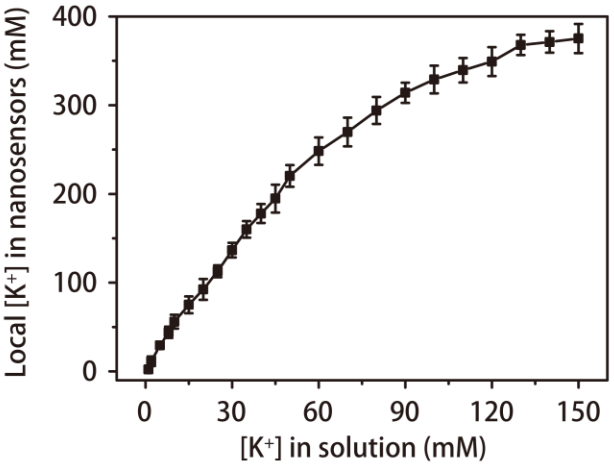

Fig. S6. ICP measurements of local [K^+] in the mesopores when the shielded nanosensors were dispersed in solutions with various [K^+]. When the shielded nanosensors were dispersed in the solution with various [K^+], local [K^+] in the mesopores was significantly higher than [K^+] in the solution, indicating the strong attraction effect of the shielded nanosensors.

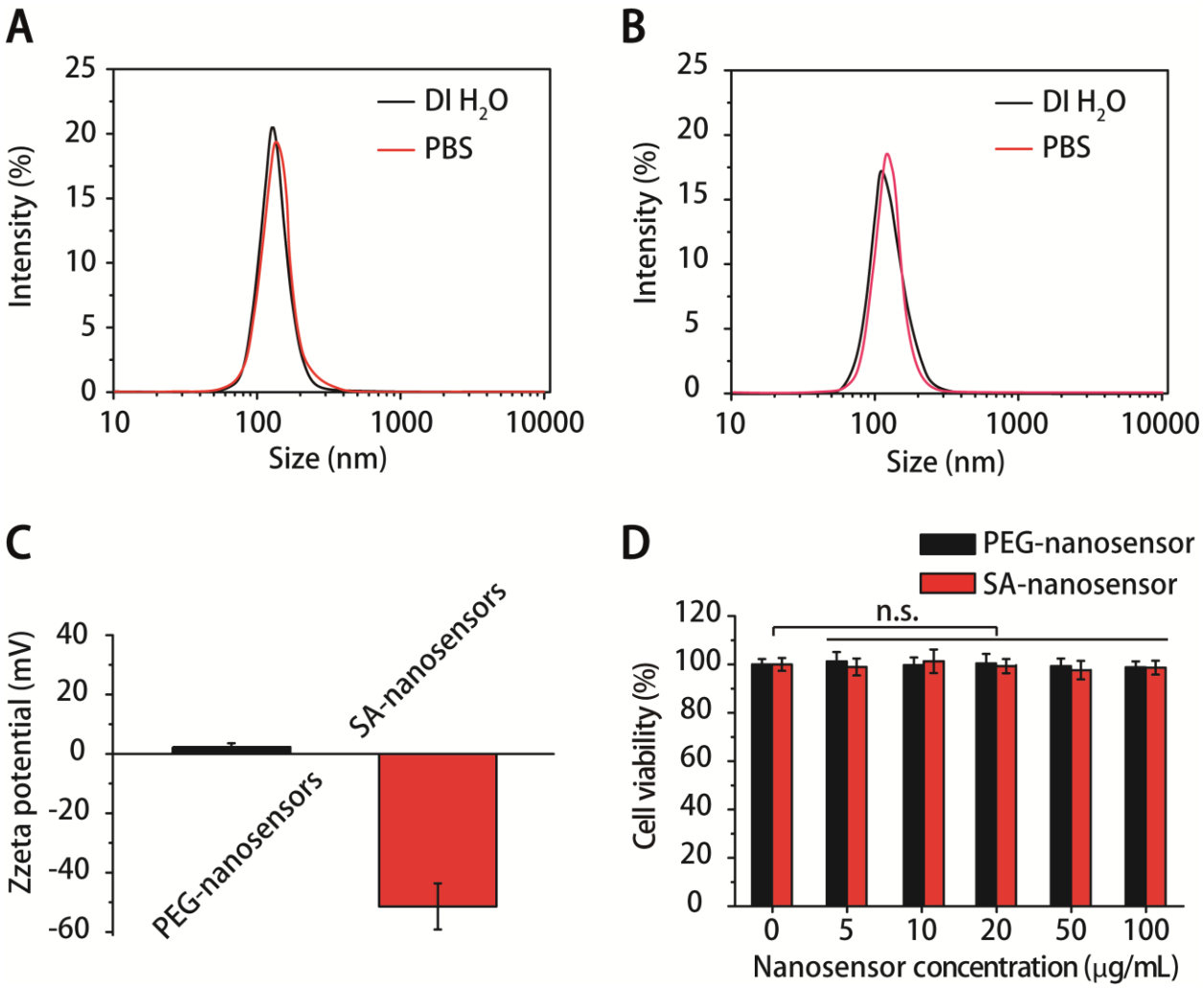

Fig. S7. Evaluation of the stability and biocompatability of the surface-modified nanosensors. (A and B) Size distribution of the surface-modified nanosensors in water and PBS measured by dynamic light scattering. No aggregation was observed for PEG-nanosensor (A), streptavidin-conjugated nanosensors (B, designated as SA-nanosensor) in either water or PBS solution. **(C)** Zeta potential of the surface-modified nanosensors (mean ± SD; n = 6 samples × 3 replicate). Nanoparticle of 0.1 nM was dispersed in DI H_2O. **(D)** Cell viability of HEK 293 cells incubated with the surface-modified nanosensor for 3 h at varied concentrations. The cell viability remained higher than 95% in each case, indicating a good cellular compatibility of the nanosensor. The experiments were performed in sextuplicate in 96-well microplates (n = 6 per group), mean ± s.d.

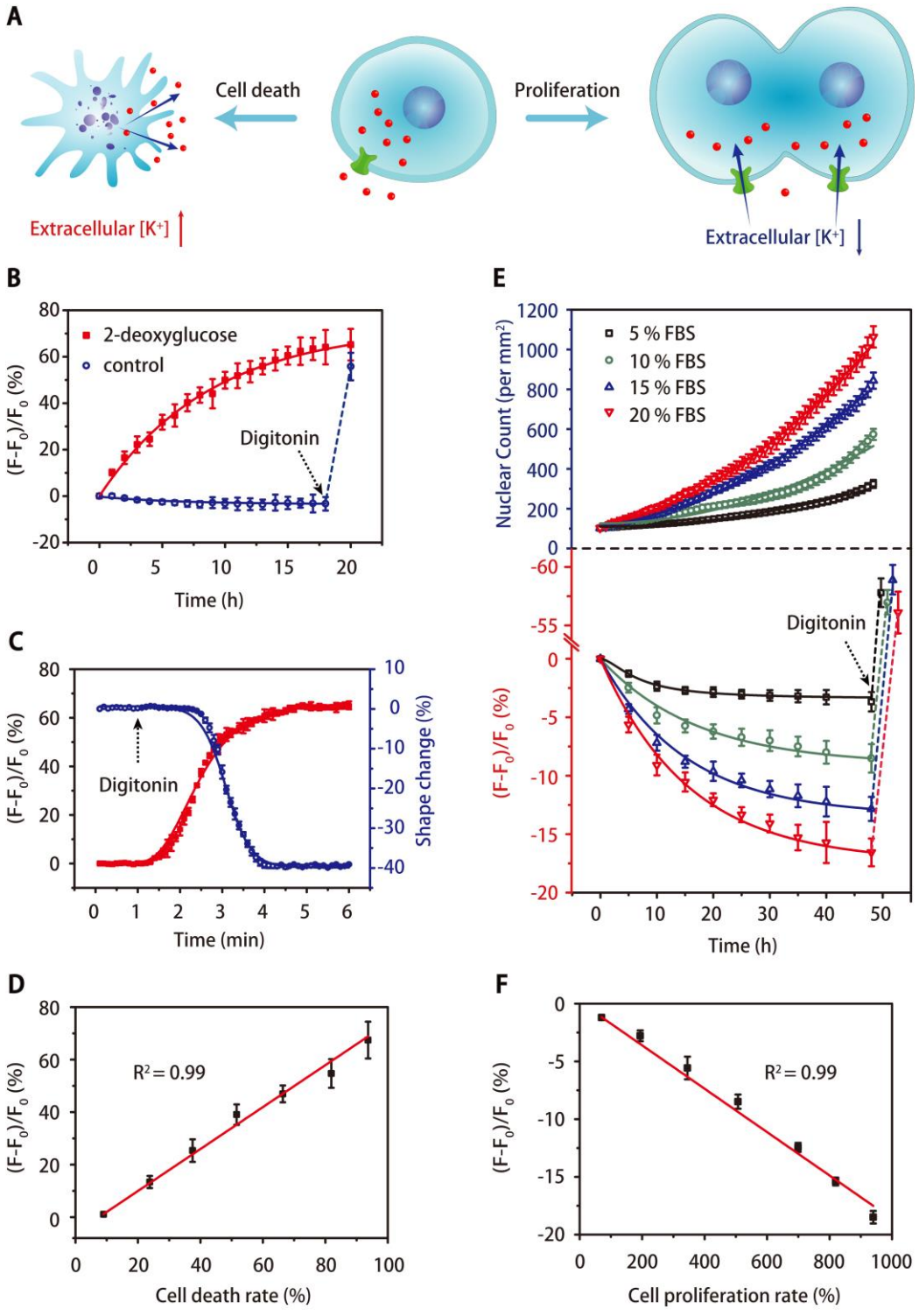

Fig. S8. Nanosensor-assisted determination of cell death and proliferation rate. **(A)** Schematic illustration of cellular K^+ loss (left arrow) and uptake (right arrow) upon cell death and proliferation, respectively. **(B)** Nanosensor-assisted determination of extracellular [K^+] of

HEK 293 cells cultured with either 10 mM 2-deoxyglucose (red squares and line, n = 6 ± SD) DMEM or (blue circles and line, n = 6 ± SD) over time. As indicated, 50 μM digitonin was applied after 18 h. **(C)** Simultaneous recording of nanosensor's optical signal (upper red curve) in the extracellular region and morphological alterations (cell shrinkage, lower blue curve) of cells over time. As indicated, 30 μM digitonin was added to induce cell necrosis. **(D)** The increase of extracellular [K^+] was determined by nanosensors along with the cell death. **(E)** Nanosensor-assisted determination of extracellular [K^+] of HEK 293 cells incubated with different culture mediums containing 5%, 10%, 15%, and 20% FBS, respectively. Cell nuclear counts were performed on a fluorescence microscope (upper curve). The optical intensity of extracellular-located nanosensors were recorded at different time points during proliferation (bottom curve). As indicated, 50 μM digitonin was applied after 48 h. **(F)** The decrease of extracellular [K^+] was determined by nanosensors along with the cell proliferation.

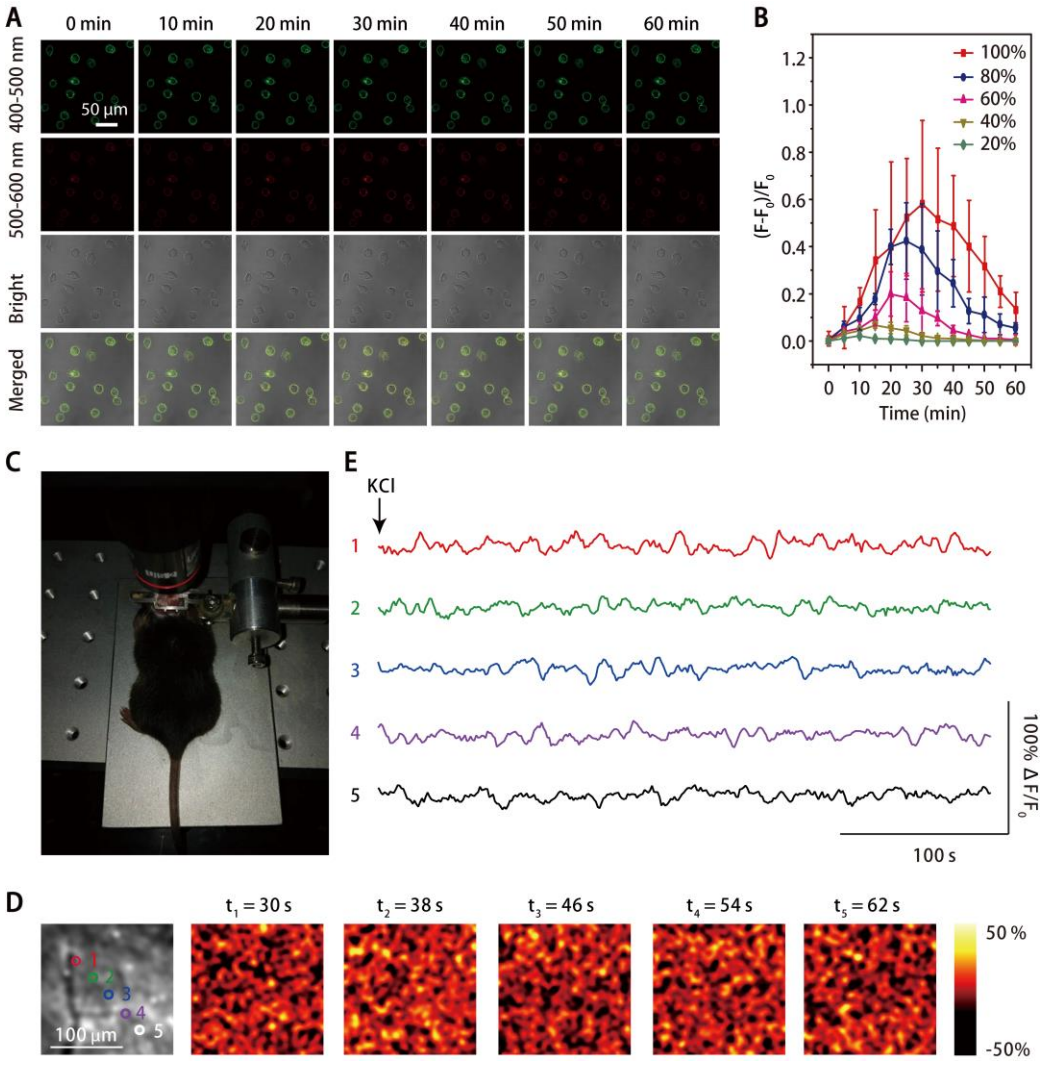

Fig. S9. In vitro and in vivo results on the unshielded nanosensor. **(A)** Fluorescence imaging obtained using CLSM shows the fluorescence changes of unshielded nanosensor-labeled HEK 293 cells upon the treatment with a mixture of nigericin, bumetanide, and ouabain for 0, 10, 20, 30, 40, 50, and 60 min. **(B)** Time-dependent fluorescence fluctuations of unshielded nanosensor-labeled HEK 293 cells after treatments with different concentrations (20%, 40%, 60%, 80%, and 100%) of K^+ efflux stimulator. **(C)** Digital photograph of the mouse during NIR imaging experiments. Photo Credit: Jianan Liu, Institute of Neuroscience, Chinese Academy of Sciences, Shanghai China. **(D)** Fluorescence images of the brain cortex at the indicated time points after initiating spreading depression. Nanosensor fluorescence is in pseudo-color. Different locations are marked with color circles. **(E)** Expanded time courses from locations indicated by colored circles in D. Each group was repeated in five independent cultures or mice.

Legend for Movie S1:

K^+ imaging results of the shielded nanosensors-treated mouse brain upon initiating spreading depression by KCl triggering. The video is eight times faster than the real speed.